Efficient Path Planning for UAVs to Recognize Chimneys with Excessive Exhaust Emissions

You-Chiun Wang and Che-Yi Chen

Abstract—The severity of air pollution has prompted increased attention to air pollution monitoring. This paper uses *unmanned aerial vehicles (UAVs)* to discover chimneys with excessive exhaust emissions (called *3E-chimneys*) in an industrial area. An efficient path-planning framework is proposed to find the flight path of a UAV for checking out chimneys and determine *sampling points (SPs)* to collect data. The framework builds the shortest path to visit chimneys. Four schemes are designed to select SPs around each chimney. The *dual-location sampling (DLS)* scheme chooses two SPs for each chimney according to its height. The *upward spiral sampling (USS)* scheme lets the UAV spiral upward at each chimney to gather data. In the *inverted-U sampling (IUS)* scheme, the UAV flies up to visit downwind SPs and then flies down to pass upwind SPs. The *asynchronous isometric sampling (AIS)* scheme picks an upwind SP and multiple downwind SPs. On doing the monitoring task, the UAV checks if some chimneys are skippable (i.e., not 3E-chimneys) using the *industrial source complex (ISC3)* model. In this way, the UAV can expedite the monitoring task and save energy. Simulation results reveal that the AIS scheme strikes a good balance between cost and performance for the monitoring task. The cost is defined by the length of the UAV's flight path. Four metrics are adopted to evaluate the performance: accuracy, recall, precision, and F1-score. Moreover, we make a prototype system to show the feasibility of our framework, which measures the concentration of CO_2 gases emitted from small chimneys in a micro-field with a single wind direction to recognize 3E-chimneys.

Index Terms—Air pollution, chimney, industrial source complex (ISC3), path planning, unmanned aerial vehicle (UAV).

1 Introduction

Air pollution is a global problem caused by air pollutants harmful to the ecosystem and people, like CO_2, NO_2, SO_2, O_3, and *particulate matter (PM)*. Factories, automobiles, and forest fires are pollution sources. The World Health Organization indicates that 99% of the global population breathes air that exceeds guideline limits and contains high levels of pollutants [1]. Hence, people pay more and more attention to air pollution. How to efficiently collect data on air quality and monitor air pollution is a critical issue.

In the past, air pollution monitoring was done by installing expensive, static monitoring stations on dedicated sites, which provided a large-range assessment of air quality. However, this method has three drawbacks [2]. First, since only a few stations are employed, the spatial resolution of air pollution sampling would be poor. Second, using static stations lacks flexibility, as some sites to deploy stations may become superfluous (e.g., factories abandoned as a city grew) or be affected by weather (e.g., changes in seasonal winds). Third, it incurs a high cost to move the stations to support dynamic monitoring tasks, for example, detecting air pollution in a suspicious area.

Unmanned aerial vehicles (UAVs) are a mature technology that has been applied in many fields (e.g., search and rescue, precision agriculture, and surveillance) [3]. UAVs carry multiple sensing devices to collect data and wireless transceivers for communications. Compared to ground-based sensors, using UAVs as flying platforms for sensors brings many benefits, including offering 3D monitoring, adjusting altitude, bypassing obstacles, and quickly reaching destinations [4].

This paper locates air pollution sources via UAVs, focusing on chimneys with excessive exhaust emissions (referred to as *3E-chimneys*) in an industrial area. The ISC3 (industrial source complex, version 3) model [5] is applied to assess pollutant dispersion in the air. We develop a path-planning framework to schedule the UAV's flight path and select *sampling points (SPs)* for it to collect data at each chimney. The framework creates the shortest path to visit chimneys and then singles out SPs using four schemes that consider air pollutant dispersion. The *dual-location sampling (DLS)* scheme finds two SPs for each chimney based on its height. The *upward spiral sampling (USS)* scheme asks the UAV to fly along an upward spiral to gather data. The *inverted-U sampling (IUS)* scheme makes the UAV fly up to pass *downwind (DW)* SPs and fly down to visit *upwind (UW)* SPs. The *asynchronous isometric sampling (AIS)* scheme picks a UW SP and some DW SPs. With ISC3, the UAV checks if some chimneys can be skipped (i.e., not 3E-chimneys) to reduce the task execution time and save energy.

Through simulations, we measure the cost and performance with which the UAV conducts its monitoring task. The cost is defined as the length of the UAV's flight path. Four metrics are used to measure performance: accuracy, recall, precision, and F1-score. To show the feasibility of our path-planning framework, we made a prototype by integrating sensing devices and a ZigBee module on an Arduino board. The prototype is used to monitor the concentration of CO_2 gases emitted from small chimneys in a micro-field with one single wind direction for identifying 3E-chimneys.

Our contributions are threefold:

- We study the problem of searching for pollution sources (i.e., 3E-chimneys). This is important to pollution control (as we can stop 3E-chimneys from continuing to pollute) but has not been efficiently addressed yet.
- Our framework takes air pollutant dispersion into account (based on ISC3), so it can select suitable positions for a UAV to sample data to identify 3E-chimneys. Do-

The authors are with the Department of Computer Science and Engineering, National Sun Yat-sen University, Kaohsiung 80424, Taiwan (e-mail: ycwang@cse.nsysu.edu.tw; joey19961230@gmail.com).

ing so facilitates the UAV's execution of the monitoring task.
- Unlike existing solutions, which aim to reduce the UAV's flight path, our framework shortens the path while keeping the recognition accuracy of 3E-chimneys. Thus, it can strike a good balance between cost and performance.

The rest of this paper is organized as follows: Section 2 depicts ISC3, Section 3 surveys related work, and Section 4 defines the problem. We propose the path-planning framework in Section 5. Sections 6 and 7 give the simulation study and prototyping experience. Section 8 concludes this paper.

2 ISC3 Pollutant Dispersion Model

ISC3 is one variation of the Gaussian plume model used to formulate how pollutants diffuse and settle in the air. It takes account of various emission sources, such as point, line, area, and volume sources. ISC3 can analyze many characteristics of pollutants, including the downwash effect, both sedimentation and dry deposition of particles, and limited terrain adjustment.

The Pasquill stability category has seven classes that represent atmospheric turbulence [6]: (A) extremely unstable, (B) moderately unstable, (C) slightly unstable, (D) neutral, (E) slightly stable, (F) moderately stable, and (G) extremely stable. Here, we adopt class E for a general case.

Let an emission source of *exhaust gas (EG)* be located at the origin. Then, the pollutant concentration at a position (x, y, z) in the 3D space can be assessed as follows:

$$\vartheta(x, y, z) = (Q_i B \varphi_y \varphi_z)/\mu, \tag{1}$$

where Q_i denotes the EG emission rate, B is a coefficient for disintegration (used when the pollutant has a half-life period, like SO_2), and μ is the wind speed. In Eq. (1), φ_y and φ_z are dilution factors in horizontal and vertical directions:

$$\varphi_y = \frac{\exp\left[-y^2/2\sigma_y^2\right]}{\sqrt{2\pi}\sigma_y}, \qquad \varphi_z = \frac{\exp\left[-(z-h)^2/2\sigma_z^2\right] + \exp\left[-(z+h)^2/2\sigma_z^2\right]}{\sqrt{2\pi}\sigma_z}, \tag{2}$$

where h is the height of a smoke plume. Moreover, σ_y and σ_z are dispersion parameters in horizontal and vertical directions:

$$\sigma_y = \frac{\varepsilon_1 x}{(1+\varepsilon_2 x)^{\varepsilon_3}} \quad \text{and} \quad \sigma_z = \frac{\varepsilon_4 x}{(1+\varepsilon_5 x)^{\varepsilon_6}}. \tag{3}$$

For class E, we set empirical constants as $\varepsilon_1 = 0.11$, $\varepsilon_2 = 0.004$, $\varepsilon_3 = 0.5$, $\varepsilon_4 = 0.08$, $\varepsilon_5 = 0.0015$, and $\varepsilon_6 = 0.5$.

The plume's height h depends on the chimney's height h_i, the downwash effect Δ_{W}, and the rise Δ_{R} in the plume:

$$h = h_i + \Delta_{\mathrm{W}} + \Delta_{\mathrm{R}}. \tag{4}$$

Let v_i be the *gas exit velocity (GEV)*, the speed at which gases leave a chimney. If $v_i < 1.5\mu$, the downwash effect will occur, which can be estimated by $\Delta_{\mathrm{W}} = 4r_i(v_i/\mu - 1.5)$, where r_i is the chimney's radius.

Two methods are used to measure the rise in the plume. In the *buoyancy-dominated* method, the rise is estimated by

$$\Delta_{\mathrm{R}} = \sqrt[3]{(F_{\mathrm{b}} x^2)/\mu_{\mathrm{G}}^3}, \tag{5}$$

where μ_{G} denotes the wind speed at ground level. In Eq. (5), F_{b} is a parameter for buoyancy flux. More specifically, $F_{\mathrm{b}} = (1 - \rho_s/\rho) g r_i^2 v_i$, where ρ_s is the density of target gas, ρ is the density of ambient air, and g is the gravitational acceleration ($g = 9.8\,\mathrm{m/s^2}$). In the *momentum-dominated* method, the rise is calculated by

$$\Delta_{\mathrm{R}} = (3F_{\mathrm{m}} \times \sin(x\sqrt{\Omega}/\mu))/(\lambda\mu\sqrt{\Omega}). \tag{6}$$

Here, Ω is a stability parameter, $\lambda = 1/3 + \mu/v_i$, and F_{m} is a parameter for momentum flux, where $F_{\mathrm{m}} = (\rho_s/\rho) r_i^2 v_i^2$.

Let T_s and T_a denote the temperatures of the target gas and ambient air, respectively. We compute their difference ΔT and the crossover temperature difference T_c:

$$\Delta T = T_s - T_a \quad \text{and} \quad T_c = 0.015982 \times T_s v_i \sqrt{\Omega}. \tag{7}$$

The stability parameter is derived by $\Omega = \varepsilon_7 \times g/T_a$, where ε_7 is an empirical constant (usually set to 0.02). Based on ΔT and T_c, we can decide which method is used to measure rise Δ_{R} in the plume. If $\Delta T > T_c$, the buoyancy-dominated method is used; otherwise, we adopt the momentum-dominated method.

3 Related Work

In this section, we divide related work into three categories: 1) deploying static sensor networks to monitor air quality; 2) performing air quality monitoring with the help of pedestrians and cars; and 3) using UAVs to detect air pollution.

3.1 Monitoring Using Static Sensor Networks

The study [7] measured PM concentration by sensors. Data from sensors was stored on a Raspberry Pi and sent to a server via Wi-Fi. Li et al. [8] developed a PM2.5 monitoring system. They placed sensors based on local weather, terrain, and land use. The work [9] investigated the optimal sensor deployment to capture pollution coverage with different weather conditions and ensure network connectivity. Sun et al. [10] placed multi-type sensors to monitor air quality in a Gaussian spatial field. They considered placing all types of sensors or at least one type of sensor on each chosen site.

Some studies predicted air quality. Four regression methods were employed in [11] for prediction: decision tree, random forest, gradient boosting, and neural network. With a machine learning method called CatBoost, the work [12] forecasted air quality and warned people of the upcoming severe pollution.

However, using static sensor networks to monitor air pollution has two disadvantages [13]. First, it requires deploying many sensors to collect data, incurring a high cost. Second, the sensor network cannot be directly reused when the monitoring task is moved to another place.

3.2 Monitoring with the Help of Pedestrians and Cars

Mobile crowdsensing relies on population density to monitor environments. Without deploying sensor networks, pedestrians carry mobile devices with sensors for monitoring [14]. Dutta et al. [15] designed a monitoring system to let people share collected data in the cloud, allowing them to view pollution footprints and air quality. In [16], pedestrians carried sensors to measure the temperature, humidity, and air pollutants. Sensing data was used to draw air quality and temperature maps. A personal monitoring system was used in [17] to observe polluted gases (e.g., NO_2), ultraviolet intensity, and ambient noises. In [18], a set of locations were chosen for pedestrians to sample data. The concentration of air pollution in unselected locations was inferred by compressive sensing.

TABLE 1: Comparison between the prior work using UAVs for monitoring air pollution and our work (GP: Gaussian plume).

work	dispersion model	source finding	SP selection	path reduction	monitoring accuracy
[25]			√		
[26]			√		√
[27]	GP		√		√
[28]		√	√		√
[29]			√		
[30]					
[31]	GP	√	√	√	
ours	ISC3	√	√	√	√

Equipping cars with sensors to monitor air quality has been discussed. The study [19] proposed two sensing scenarios: 1) buses moved on fixed routes to gather data, and 2) drivers put sensors on cars to monitor air quality. Hu et al. [20] used cars to carry sensors to monitor CO, NO_2, and O_3 concentration. Roadside monitors helped calibrate the readings of sensors on cars. In [21], static sensors provided a whole view of air quality, while mobile sensors (by cars) gathered more accurate data on designated locations. Both [22] and [23] divided a monitoring area into grids and adjusted the reporting rates of cars in each grid to save on message costs and maintain monitoring accuracy. Chen et al. [24] exploited spatiotemporal correlation in the distribution of air pollutants to derive values at non-sensed locations in areas with sparse data.

However, the above methods have some limitations. First, the mobility of pedestrians and cars is uncontrollable. Asking them to move to specific locations to sample data is difficult. Second, some places are inaccessible to pedestrians and cars (e.g., hazardous or prohibited regions). Third, these methods provide only 2D monitoring of air quality. Some applications, like finding 3E-chimneys, require 3D monitoring.

3.3 Monitoring Using UAVs

Using UAVs to carry sensors for monitoring conquers the limitations mentioned in Section 3.2. They can fly to places not reachable by pedestrians or cars and offer 3D monitoring. In [25], a UAV carrying sensors flew to measure the concentration of air pollutants. The study [26] took aerial panoramic images using a UAV and estimated an *air quality index (AQI)* using the haze pictures. Yang et al. [27] designed a Gaussian plume model based on the neural network to describe particle dispersion and collected data via a UAV to draw AQI maps. Chhikara et al. [28] proposed a federated learning scheme for a swarm of UAVs to monitor air quality. Sensing data was fed to a convolutional neural network to predict AQI. Hu et al. [29] proposed an air quality monitoring system using ground and UAV sensors. Hoque et al. [30] put IoT devices on UAVs to support monitoring services (e.g., detecting air pollution).

Le et al. [31] adopted UAVs to find 3E-chimneys with the minimum search time. They picked two SPs for each chimney, whose heights were computed using a Gaussian plume model. To save the search time, an interference graph was employed to remove some chimneys from the UAV's visiting list. This method, called the *interference graph-based algorithm (IGBA)*, has to know the GEV of each chimney to get the right height for its SPs. Nevertheless, GEVs cannot be known in practice, which may cause inaccurate monitoring results.

Table 1 compares the prior work using UAVs for monitoring air pollution with our work. To estimate air pollutant dispersion, both [27] and [31] employ Gaussian plume models, while our work adopts the ISC3 model (suitable for industrial areas). For source finding, the work [28] identifies the region with the highest AQI. Both [31] and our work search for 3E-chimneys. Except for [30], others select SPs for UAVs to gather data. As can be seen, the prior work considers either reducing the UAV's flight path or raising monitoring accuracy. Compared to them, our work takes both path reduction and monitoring accuracy into consideration. This distinguishes our work from the prior work and presents the novelty of our work.

4 Problem Formulation

We are given a set $\hat{\mathcal{C}}$ of n chimneys in the industrial area with no obstacles or buildings higher than the lowest chimney in $\hat{\mathcal{C}}$. Each chimney $c_i \in \hat{\mathcal{C}}$ is modeled as one cylinder with a height of h_i and a radius of r_i. Moreover, c_i's location is a given parameter. The weather is sunny, and there is a stable and unidirectional wind source with a speed of μ. Chimney c_i emits EG at an unknown rate (denoted by Q_i). If $Q_i > Q_{\mathtt{th}}$, c_i is a 3E-chimney, where $Q_{\mathtt{th}}$ is the statutory threshold.

To identify 3E-chimneys in $\hat{\mathcal{C}}$, a UAV ψ carrying gaseous sensors flies to check out chimneys and sends the collected data to a nearby ground station for analysis[1]. As EG emitted from chimneys may be caustic or have a high temperature, ψ cannot be right above or very close to a chimney. Instead, ψ shall be away from each chimney at a *minimum safe distance* $d_{\mathtt{MS}}$ to avoid damage.

Depending on the judgment and the true answer, the monitoring result for each chimney $c_i \in \hat{\mathcal{C}}$ has four combinations: 1) *True positive*: c_i is judged as a 3E-chimney, and it indeed is. 2) *True negative*: c_i is judged as not a 3E-chimney, and it indeed is not. 3) *False positive*: c_i is judged as a 3E-chimney, but it actually is not. 4) *False negative*: c_i is judged as not a 3E-chimney, but it actually is. Let $f_{\mathtt{TP}}$, $f_{\mathtt{TN}}$, $f_{\mathtt{FP}}$, $f_{\mathtt{FN}}$ be the number of true positives, true negatives, false positives, and false negatives for the monitoring results of all chimneys.

Then, our problem asks how to find a set $\hat{\mathcal{P}}_i$ of SPs for each chimney c_i and decide a flight path Γ for UAV ψ such that the cost of the monitoring task is minimized and the performance is maximized. It can be expressed mathematically as follows:

$$\text{minimize} \quad \tilde{L}(\Gamma), \tag{8}$$

$$\text{maximize} \quad (f_{\mathtt{TP}} + f_{\mathtt{TN}})/(f_{\mathtt{TP}} + f_{\mathtt{TN}} + f_{\mathtt{FP}} + f_{\mathtt{FN}}), \tag{9}$$

$$\text{maximize} \quad \Lambda_{\mathbf{R}} = f_{\mathtt{TP}}/(f_{\mathtt{TP}} + f_{\mathtt{FN}}), \tag{10}$$

$$\text{maximize} \quad \Lambda_{\mathbf{P}} = f_{\mathtt{TP}}/(f_{\mathtt{TP}} + f_{\mathtt{FP}}), \tag{11}$$

$$\text{maximize} \quad 2(\Lambda_{\mathbf{R}} \times \Lambda_{\mathbf{P}})/(\Lambda_{\mathbf{R}} + \Lambda_{\mathbf{P}}) \tag{12}$$

subject to

$$h_{\min} \le h_i \le h_{\max}, \qquad \forall c_i \in \hat{\mathcal{C}}, \tag{13}$$

$$r_{\min} \le r_i \le r_{\max} \qquad \forall c_i \in \hat{\mathcal{C}}, \tag{14}$$

$$v_{\min} \le v_i \le v_{\max}, \qquad \forall c_i \in \hat{\mathcal{C}}, \tag{15}$$

$$Q_{\min} \le Q_i \le Q_{\max} \qquad \forall c_i \in \hat{\mathcal{C}}, \tag{16}$$

$$\text{distance}(\psi, c_i) \ge r_i + d_{\mathtt{MS}}, \qquad \forall c_i \in \hat{\mathcal{C}}, \tag{17}$$

$$z_i \in \{0, 1\}, \qquad \forall c_i \in \hat{\mathcal{C}}, \tag{18}$$

$$|\hat{\mathcal{P}}_i| \ge 1 \text{ if } z_i = 1, \qquad \forall c_i \in \hat{\mathcal{C}}, \tag{19}$$

$$\text{distance}(p_j, c_i) \ge r_i + d_{\mathtt{MS}}, \qquad \forall p_j \in \hat{\mathcal{P}}_i, \forall c_i \in \hat{\mathcal{C}}. \tag{20}$$

1. Refer to [32] for how to offer reliable communications between the UAV and ground stations.

TABLE 2: Summary of acronyms and notations.

(a) Summary of acronyms

acronym	full name
3E-chimney	chimney with excessive exhaust emissions
AIS	asynchronous isometric sampling
DLS	dual-location sampling
DW/UW	downwind/upwind
EG	exhaust gas
GEV	gas exit velocity
IGBA	interference graph-based algorithm
ISC3	industrial source complex (version 3)
IUS	inverted-U sampling
SP	sampling point
TSP	traveling salesman problem
UAV	unmanned aerial vehicle
USS	upward spiral sampling

(b) Summary of notations

notation	definition
$\hat{\mathcal{C}}$	set of chimneys in the industrial area ($\lvert\hat{\mathcal{C}}\rvert = n$)
$\hat{\mathcal{P}}_i^{\mathtt{D}}, \hat{\mathcal{P}}_i^{\mathtt{U}}$	sets of DW and UW SPs for chimney c_i ($\hat{\mathcal{P}}_i^{\mathtt{D}} \cup \hat{\mathcal{P}}_i^{\mathtt{U}} = \hat{\mathcal{P}}_i$)
h_i, r_i	height and radius of c_i
Q_i, $Q_{\mathtt{th}}$	c_i's EG emission rate and the statutory threshold
$d_{\mathtt{MS}}$	minimum safe distance
h_s	distance between two adjacent SPs in $\hat{\mathcal{P}}_i^{\mathtt{D}}$ or $\hat{\mathcal{P}}_i^{\mathtt{U}}$
μ	wind speed
m	number of pairs of DW/UW SPs in USS and IUS
p_0	point of departure of UAV ψ
$p_x \rightarrow p_y$	straight line between two points p_x and p_y
$p_x \curvearrowright p_y$	circular arc between p_x and p_y (radius: $r_i + d_{\mathtt{MS}}$)
$p_x \rightsquigarrow p_y$	an upward spiral from p_x to p_y
$\tilde{L}(\cdot)$	length of a path
$\Gamma_{\mathtt{IC}}$, Γ_i	inter-chimney path and the path to visit SPs in $\hat{\mathcal{P}}_i$
$\tilde{h}$	maximum height difference between two chimneys
$\tilde{d}$	maximum distance between two adjacent chimneys

In Eq. (8), the objective is to minimize ψ's flight path (i.e., cost), where $\tilde{L}(\cdot)$ signifies the length of a path. The objectives in Eqs. (9), (10), (11), and (12) are to maximize the accuracy, recall, precision, and F1-score (i.e., performance metrics). For constraints, Eqs. (13) and (14) put upper and lower bounds on the height and radius of each chimney c_i, where h_i and r_i are given parameters. Eqs. (15) and (16) impose upper and lower bounds on c_i's GEV and EG emission rate, where v_i and Q_i are unknown. Eq. (17) gives the constraint of a minimum safe distance. In Eq. (18), variable z_i is used to indicate whether c_i is scheduled to be visited by ψ. If so, $z_i = 1$; otherwise, $z_i = 0$. Eq. (19) means that if c_i is visited by ψ, at least one SP shall be chosen. In Eq. (20), the choice of each SP must consider the constraint of a minimum safe distance.

Table 2 summarizes the acronyms and notations.

Remark 1 (Multiple UAVs). Though our discussion aims at one UAV, it can be extended to the case of multiple UAVs. To do so, we divide all chimneys in $\hat{\mathcal{C}}$ into groups using K-means, such that the number of groups is equal to the number of UAVs. Then, each UAV takes charge of checking out the chimneys in a group. Since the chimneys in each group would be close to each other (due to the property of K-means [33]), the flight path of each UAV can be reduced.

Remark 2 (Wardens). Some studies [34], [35] consider hindering wardens (i.e., adversaries) from detecting data transmissions of UAVs via the technique of covert communication. Our work aims to utilize UAVs to collect data for finding 3E-chimneys, not to provide secure communications for UAVs. Hence, how to resist the attacks of wardens is out of the paper's scope. We will leave this issue for future work.

5 The Proposed Path-Planning Framework

Given the point of departure p_0 of UAV ψ, the path-planning framework contains five steps:

1. Create the shortest path $\Gamma_{\mathtt{S}}$ for ψ to start from p_0, visit all chimneys in $\hat{\mathcal{C}}$, and return to p_0.

2. For each chimney $c_i \in \hat{\mathcal{C}}$, we find a set $\hat{\mathcal{P}}_i$ of SPs for ψ to collect data and decide a path Γ_i to visit SPs in $\hat{\mathcal{P}}_i$.

3. UAV ψ checks out chimneys based on the sequence on $\Gamma_{\mathtt{S}}$. On visiting a chimney c_i, ψ flies on path Γ_i and gathers data at each SP in $\hat{\mathcal{P}}_i$.

4. Let c_j be the next chimney to be visited. UAV ψ checks if c_j is *not* a 3E-chimney using the ISC3 model. If so, ψ skips c_j and visits its next chimney. Otherwise, ψ flies to visit c_j.

5. Repeat steps 3 and 4 until each chimney in $\hat{\mathcal{C}}$ has been visited or skipped.

In step 1, we can employ an approximation solution to the *traveling salesman problem (TSP)* [36] to compute path $\Gamma_{\mathtt{S}}$. For steps 2 and 3, we propose four sampling schemes to find set $\hat{\mathcal{P}}_i$ of SPs and decide path Γ_i, namely the DLS, USS, IUS, and AIS schemes, as detailed in Sections 5.1, 5.2, 5.3, and 5.4, respectively. Regarding step 4, we discuss how to judge whether a chimney can be skipped in Section 5.5.

Suppose that $\hat{\mathcal{C}}'$ is the set of chimneys skipped by step 4. The solution set of SPs is $\bigcup_{c_i \in \hat{\mathcal{C}} \setminus \hat{\mathcal{C}}'} \hat{\mathcal{P}}_i$. Let $\Gamma'_{\mathtt{S}}$ be the updated shortest path by removing the chimneys in $\hat{\mathcal{C}}'$ from $\Gamma_{\mathtt{S}}$. The final flight path for UAV ψ will be

$$\Gamma = \Gamma_{\mathtt{IC}} \cup \{\Gamma_i \mid \forall c_i \in \hat{\mathcal{C}} \setminus \hat{\mathcal{C}}'\}, \tag{21}$$

where $\Gamma_{\mathtt{IC}}$ is the inter-chimney path. It is the union of 1) the path from p_0 to the first SP of the first chimney on $\Gamma'_{\mathtt{S}}$, 2) each path from the last SP of a chimney to the first SP of its next chimney on $\Gamma'_{\mathtt{S}}$, and 3) the path from the last SP of the last chimney on $\Gamma'_{\mathtt{S}}$ to p_0. Then, Section 5.6 discusses the design rationale and the computational complexity. In Section 5.7, we analyze the distance between each sampling scheme (i.e., a suboptimal solution) and the optimal solution.

5.1 Dual-Location Sampling (DLS) Scheme

Air pollutants spread from the UW side to the DW side, so UAV ψ shall fly from the DW side to the UW side. Fig. 1(a) shows candidate SPs for ψ to collect data around a chimney c_i. We select a set $\hat{\mathcal{P}}_i^{\mathtt{D}}$ of DW SPs, where each SP $p_{i,a}^{\mathtt{D}} \in \hat{\mathcal{P}}_i^{\mathtt{D}}$ is on c_i's DW side and has a distance $d_{\mathtt{MS}}$ from the boundary extension line of c_i, as shown by the yellow dots in Fig. 1(a). The distance between two adjacent SPs in $\hat{\mathcal{P}}_i^{\mathtt{D}}$ is h_s. Moreover, we choose a set $\hat{\mathcal{P}}_i^{\mathtt{U}}$ of UW SPs, where each SP $p_{i,b}^{\mathtt{U}} \in \hat{\mathcal{P}}_i^{\mathtt{U}}$ is on c_i's UW side and has a distance $d_{\mathtt{MS}}$ from the boundary extension line of c_i, as shown by the blue dots in Fig. 1(a). The distance between two adjacent SPs in $\hat{\mathcal{P}}_i^{\mathtt{U}}$ is h_s.

To avoid being damaged by EG, as UAV ψ flies from a DW SP $p_{i,a}^{\mathtt{D}} \in \hat{\mathcal{P}}_i^{\mathtt{D}}$ to a UW SP $p_{i,b}^{\mathtt{U}} \in \hat{\mathcal{P}}_i^{\mathtt{U}}$, it follows a circular arc (denoted by $p_{i,a}^{\mathtt{D}} \curvearrowright p_{i,b}^{\mathtt{U}}$) whose radius is $r_i + d_{\mathtt{MS}}$. Otherwise, ψ directly flies from a point p_x to another point p_y (as denoted by $p_x \rightarrow p_y$), where a point is an SP or p_0. If there are obstacles between p_x and p_y, we can adopt the Dijkstra-based method in [37] to find the shortest path for ψ to fly from p_x to p_y that bypasses obstacles.

For chimney c_i, DLS picks a DW SP $p_{i,1}^{\mathtt{D}}$ and a UW SP $p_{i,1}^{\mathtt{U}}$ with the same height of $h_i + \Delta_{\mathtt{DLS}}$. Depending on EG, there are three cases to decide $\Delta_{\mathtt{DLS}}$. In case 1, the smoke plume trends up when EG is lighter than the air. Thus, we set $\Delta_{\mathtt{DLS}} = h_s$ to

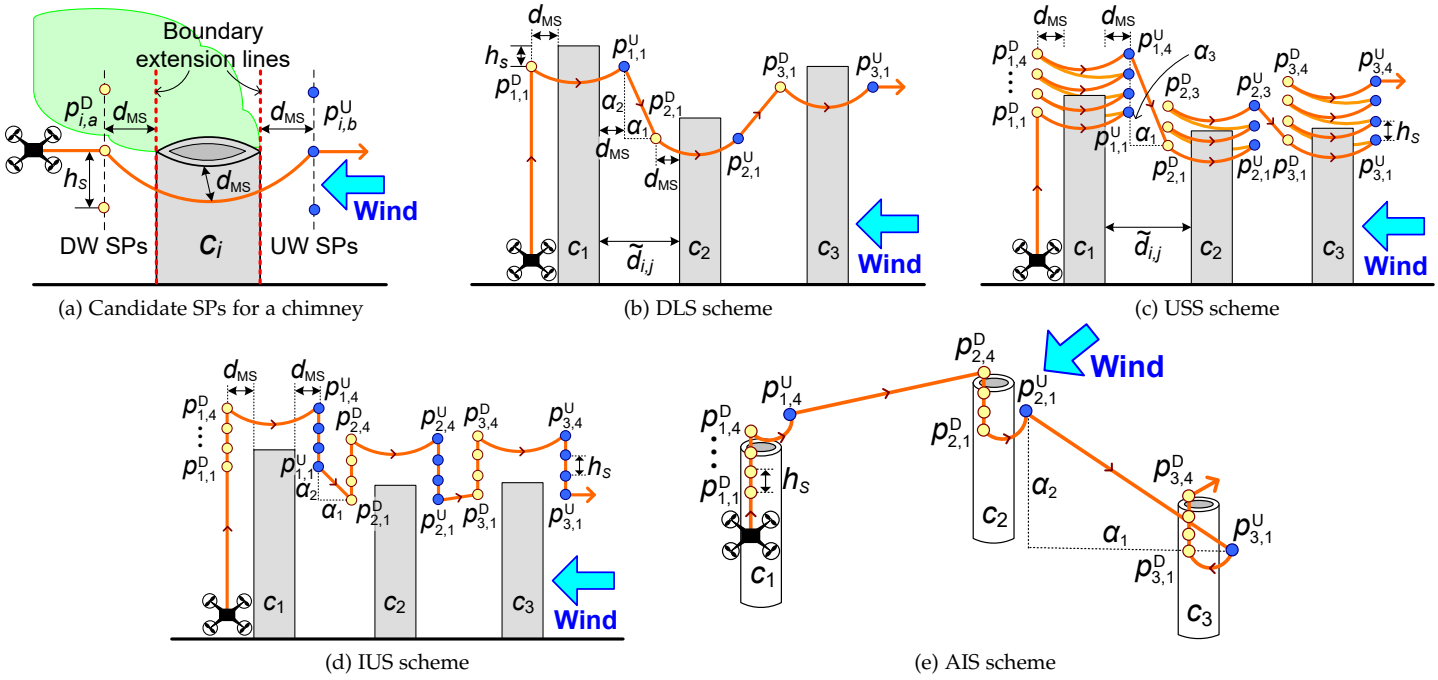

(a) Candidate SPs for a chimney (b) DLS scheme (c) USS scheme

(d) IUS scheme (e) AIS scheme

Fig. 1: Examples of our proposed sampling schemes.

make UAV ψ fly higher than c_i's height. In this way, ψ can be more likely to sample data in a region of the plume where EG concentration is high. In case 2, the plume trends down as EG is heavier than the air. Hence, we set $\Delta_{\text{DLS}} = -h_s$ to let ψ fly lower than c_i's height to help it more likely sample data at a high-concentration region of EG in the plume. In case 3, we set $\Delta_{\text{DLS}} = 0$, so ψ's flying altitude is equal to c_i's height.

Fig. 1(b) presents an example for DLS (case 2), where the visiting sequence of chimneys is $c_1 \Rightarrow c_2 \Rightarrow c_3$. The inter-chimney path is $\Gamma_{\text{IC}} = \{p_0 \to p^{\text{D}}_{1,1}\} \cup \{p^{\text{U}}_{1,1} \to p^{\text{D}}_{2,1}\} \cup \{p^{\text{U}}_{2,1} \to p^{\text{D}}_{3,1}\} \cup \{p^{\text{U}}_{3,1} \to p_0\}$. Based on Eq. (21), ψ's flight path is $p_0 \to p^{\text{D}}_{1,1} \rightsquigarrow p^{\text{U}}_{1,1} \to p^{\text{D}}_{2,1} \rightsquigarrow p^{\text{U}}_{2,1} \to p^{\text{D}}_{3,1} \rightsquigarrow p^{\text{U}}_{3,1} \to p_0$.

After collecting the EG concentration at SPs $p^{\text{D}}_{i,1}$ and $p^{\text{U}}_{i,1}$ for chimney c_i, we estimate c_i's EG emission rate Q_i. If Q_i overtakes the statutory threshold Q_{th}, c_i is judged as a 3E-chimney. The details will be discussed later in Section 5.5.

Suppose that UAV ψ visits chimneys in $\hat{\mathcal{C}}$ by a sequence of $c_{x_1} \Rightarrow c_{x_2} \Rightarrow \cdots \Rightarrow c_{x_n}$. Lemma 1 gives the maximum length of inter-chimney path Γ_{IC} in DLS, and Theorem 1 shows the maximum length of ψ's flight path when using DLS.

Lemma 1. Let $\tilde{d}$ be the maximum distance between two adjacent chimneys on path Γ_s, and let $\tilde{h}$ be the maximum difference in height between two chimneys. The maximum length of Γ_{IC} in DLS is $l^{IC}_{DLS} = (n-1)\sqrt{(\tilde{d} - 2d_{\text{MS}})^2 + \tilde{h}^2} + \beta_1$, where β_1 is the length sum of paths $p_0 \to p^{D}_{x_1,1}$ and $p^{U}_{x_n,1} \to p_0$.

Proof: Observing Fig. 1(b), the flight length between two adjacent chimneys c_i and c_j is $\tilde{L}(p^{\text{U}}_{i,1} \to p^{\text{D}}_{j,1}) = \sqrt{\alpha_1^2 + \alpha_2^2}$. We have $\alpha_1 = \tilde{d}_{i,j} - 2d_{\text{MS}}$, where $\tilde{d}_{i,j}$ is the distance between c_i and c_j. Since all chimneys have the same Δ_{DLS} value, α_2 is the height difference between c_i and c_j. The worst case is that no chimneys are skipped. Thus, we obtain that $\tilde{L}(\Gamma_{\text{IC}}) = \sum_{k=1}^{n-1} \tilde{L}(p^{\text{U}}_{x_k,1} \to p^{\text{D}}_{x_{k+1},1}) + \tilde{L}(p_0 \to p^{\text{D}}_{x_1,1}) + \tilde{L}(p^{\text{U}}_{x_n,1} \to p_0) \le (n-1)\sqrt{(\tilde{d} - 2d_{\text{MS}})^2 + \tilde{h}^2} + \beta_1$. □

Theorem 1. With DLS, UAV ψ's flight path has a length no longer than $l^{IC}_{DLS} + n\pi(r_{\max} + d_{MS})$.

Proof: The worst case is that $\hat{\mathcal{C}}' = \emptyset$ in Eq. (21) (i.e., UAV ψ has to check out every chimney). Thus, the flight length for ψ in DLS is $\tilde{L}(\Gamma_{\text{IC}}) + \sum_{k=1}^{n} \tilde{L}(p^{\text{D}}_{x_k,1} \rightsquigarrow p^{\text{U}}_{x_k,1}) = \tilde{L}(\Gamma_{\text{IC}}) + \sum_{k=1}^{n} \pi(r_{x_k} + d_{\text{MS}}) \le l^{\text{IC}}_{\text{DLS}} + n\pi(r_{\max} + d_{\text{MS}})$. □

5.2 Upward Spiral Sampling (USS) Scheme

To improve monitoring performance, USS selects m pairs of DW/UW SPs for each chimney c_i, where $m \ge 3$. The distance between two adjacent DW or UW SPs is equal. To do so, we use a vector $V = [\xi, \xi-1, \xi-2, \cdots, \xi-(m-1)]$ to determine the height of each SP, where $\xi \in \mathbb{Z}^+$ and $\xi < m-1$. The heights of the k-th pair of DW/UW SPs (i.e., $p^{\text{D}}_{i,k}$ and $p^{\text{U}}_{i,k}$) are set to $h_i - h_s \times V[k]$. Since $\xi \ge 1$, we ensure that some SPs are lower than c_i. Besides, as $\xi < m-1$, some SPs must be higher than c_i. In this way, UAV ψ can collect data in the smoke plume more comprehensively.

To gather c_i's data, beginning with SP $p^{\text{D}}_{i,1}$, UAV ψ visits DW and UW SPs alternately. Hence, path Γ_i is $p^{\text{D}}_{i,1} \rightsquigarrow p^{\text{U}}_{i,1} \rightsquigarrow p^{\text{D}}_{i,2} \rightsquigarrow p^{\text{U}}_{i,2} \rightsquigarrow \cdots \rightsquigarrow p^{\text{U}}_{i,m}$, which forms an upward spiral (as denoted by $p^{\text{D}}_{i,1} \rightsquigarrow p^{\text{U}}_{i,m}$). On flying along Γ_i, ψ compares the EG concentration sampled at each pair of DW/UW SPs and employs the method in Section 5.5 to check if c_i is a 3E-chimney. If so, there is no need to further collect c_i's data, and ψ can directly fly to the next chimney to reduce the flight path. Otherwise, ψ flies to visit the next pair of c_i's DW/UW SPs to collect data for judging c_i.

Fig. 1(c) gives an example, where $m = 4$ and $\xi = 1$. Each chimney c_i has four pairs of DW/UW SPs by default, whose heights are $h_i - h_s$, h_i, $h_i + h_s$, and $h_i + 2h_s$. Since UAV ψ infers that c_2 is a 3E-chimney after sampling data at $p^{\text{D}}_{2,3}$ and $p^{\text{U}}_{2,3}$, ψ stops collecting c_2's data and flies to c_3. That is why c_2 has only three pairs of DW/UW SPs. Then, ψ's flight path is $p_0 \to p^{\text{D}}_{1,1} \rightsquigarrow p^{\text{U}}_{1,4} \to p^{\text{D}}_{2,1} \rightsquigarrow p^{\text{U}}_{2,3} \to p^{\text{D}}_{3,1} \rightsquigarrow p^{\text{U}}_{3,4} \to p_0$.

For USS, Lemma 2 analyzes the maximum length of inter-chimney path Γ_{IC}, and Theorem 2 shows the upper bound on the length of ψ's flight path.

Lemma 2. The maximum length of Γ_{IC} in USS is $l_{USS}^{IC} = (n-1)\sqrt{(\tilde{d}-2d_{MS})^2+\varrho^2}+\beta_2$, where $\varrho = \tilde{h}+(m-1)h_s$ and β_2 is the length sum of paths $p_0 \to p_{x_1,1}^{D}$ and $p_{x_n,m}^{U} \to p_0$.

Proof: In Fig. 1(c), the flight length of UAV ψ between adjacent chimneys c_i and c_j is $\tilde{L}(p_{i,m}^{\text{U}} \to p_{j,1}^{\text{D}}) = \sqrt{\alpha_1^2+\alpha_3^2}$, where $\alpha_1 = \tilde{d}_{i,j} - 2d_{\text{MS}}$. Since each chimney has m pairs of SPs and ψ flies from c_i's last UW SP to c_j's first DW SP, we have $\alpha_3 = \tilde{h}_{i,j}+(m-1)h_s$, where $\tilde{h}_{i,j}$ is the height difference between c_i and c_j. Thus, Γ_{IC}'s length is $\tilde{L}(\Gamma_{\text{IC}}) = \sum_{k=1}^{n-1}\tilde{L}(p_{x_k,m}^{\text{U}} \to p_{x_{k+1},1}^{\text{D}}) + \tilde{L}(p_0 \to p_{x_1,1}^{\text{D}}) + \tilde{L}(p_{x_n,m}^{\text{U}} \to p_0) \le (n-1)\sqrt{(\tilde{d}-2d_{\text{MS}})^2+\varrho^2}+\beta_2$. □

Theorem 2. In USS, the length of UAV ψ's flight path is below $l_{USS}^{IC} + mn\sqrt{h_s^2+[2\pi(r_{\max}+d_{MS})]^2}$.

Proof: In USS, the worst case takes place when ψ has to sample data at each pair of DW/UW SP for all chimneys in $\hat{\mathcal{C}}$. Thus, the flight path has a length of $\tilde{L}(\Gamma_{\text{IC}}) + \sum_{k=1}^{n}\tilde{L}(p_{x_k,1}^{\text{D}} \rightsquigarrow p_{x_k,m}^{\text{U}}) = \tilde{L}(\Gamma_{\text{IC}}) + \sum_{k=1}^{n} m\sqrt{h_s^2+[2\pi(r_{x_k}+d_{\text{MS}})]^2} \le l_{\text{USS}}^{\text{IC}} + mn\sqrt{h_s^2+[2\pi(r_{\max}+d_{\text{MS}})]^2}$. □

5.3 Inverted-U Sampling (IUS) Scheme

Like USS, IUS selects m pairs of DW/UW SPs for each chimney c_i. However, instead of flying in an upward spiral, UAV ψ flies up to visit each DW SP and then flies down to visit each UW SP. In other words, path Γ_i is $p_{i,1}^{\text{D}} \to p_{i,2}^{\text{D}} \to \cdots \to p_{i,m}^{\text{D}} \curvearrowright p_{i,m}^{\text{U}} \to p_{i,m-1}^{\text{U}} \to \cdots \to p_{i,1}^{\text{U}}$, which forms an inverted-U shape. In this way, we can save the time that ψ spends hovering over each chimney and reduce its flight path.

Fig. 1(d) gives an example, where $m = 4$. The flight path is $p_0 \to p_{1,1}^{\text{D}} \to \cdots \to p_{1,4}^{\text{D}} \curvearrowright p_{1,4}^{\text{U}} \to \cdots \to p_{1,1}^{\text{U}} \to p_{2,1}^{\text{D}} \to \cdots \to p_{2,4}^{\text{D}} \curvearrowright p_{2,4}^{\text{U}} \to \cdots \to p_{2,1}^{\text{U}} \to p_{3,1}^{\text{D}} \to \cdots \to p_{3,4}^{\text{D}} \curvearrowright p_{3,4}^{\text{U}} \to \cdots \to p_{3,1}^{\text{U}} \to p_0$. Theorem 3 analyzes the maximum length of the flight path in IUS.

Theorem 3. In IUS, the length of the flight path is at most $l_{DLS}^{IC} + n(\pi(r_{\max}+d_{MS})+2(m-1)h_s)$.

Proof: Let us compare the flight paths in DLS and IUS, as shown in Fig. 1(b) and (d). They are almost the same, except that IUS makes UAV ψ additionally fly on two paths $p_{i,1}^{\text{D}} \to \cdots \to p_{i,m}^{\text{D}}$ and $p_{i,m}^{\text{U}} \to \cdots \to p_{i,1}^{\text{U}}$ for each chimney c_i. The length of each path is $(m-1)h_s$. Based on Theorem 1, the maximum length of the flight path in DLS is $l_{\text{DLS}}^{\text{IC}} + n\pi(r_{\max}+d_{\text{MS}})$. Since $\hat{\mathcal{C}}$ has n chimneys, the length of the flight path in IUS is at most $l_{\text{DLS}}^{\text{IC}} + n(\pi(r_{\max}+d_{\text{MS}})+2(m-1)h_s)$. □

Note that UAV ψ shall collect data at all DW SPs of each chimney c_i. If ψ collects data at a UW SP $p_{i,k}^{\text{U}}$ ($k > 1$) and judges that c_i is a 3E-chimney (by comparing the data collected at DW SP $p_{i,k}^{\text{D}}$), residual UW SPs (i.e., $p_{i,k-1}^{\text{U}}, \cdots, p_{i,1}^{\text{U}}$) can be skipped to reduce ψ's flight path.

5.4 Asynchronous Isometric Sampling (AIS) Scheme

Based on IUS, AIS makes two improvements: 1) decreasing SPs for each chimney without significantly degrading monitoring performance and 2) reducing the path for UAV ψ to fly from one chimney to the next.

Improvement 1. After EG is discharged from a chimney, its spreading range expands as the distance from the chimney increases. Thus, we shall choose more DW SPs to help UAV ψ collect more data within the EG's spreading range. On the other hand, the number of UW SPs can be reduced to shorten the flight path. Hence, for each chimney c_i, AIS selects m DW SPs $p_{i,1}^{\text{D}}, \cdots, p_{i,m}^{\text{D}}$ and one UW SP $p_{i,y}^{\text{U}}$, where $y = 1$ or $y = m$ (depending on ψ's flight direction on the DW side, as discussed in Improvement 2). To check if c_i is a 3E-chimney, ψ compares the EG concentration sampled at $p_{i,k}^{\text{D}}$ and $p_{i,y}^{\text{U}}$, for $k = 1...m$. In other words, the UW SP $p_{i,y}^{\text{U}}$ is taken as the reference for comparison with each DW SP.

Improvement 2. In IUS, UAV ψ always flies up on the DW side of each chimney. When there is only one UW SP, doing so may increase ψ's flight path. Take Fig. 1(e) as an example. When ψ flies from c_1 to c_2, if IUS's policy is used, ψ flies on path $p_{1,4}^{\text{U}} \to p_{2,1}^{\text{D}}$. In fact, there is a shorter path, namely $p_{1,4}^{\text{U}} \to p_{2,4}^{\text{D}}$. Hence, AIS makes two modifications:

(1) If $p_{i,1}^{\text{D}}$ is the first DW SP to be visited, ψ flies up on c_i's DW side (i.e., $p_{i,1}^{\text{D}} \Rightarrow p_{i,m}^{\text{D}}$), and we set $y = m$. Otherwise, ψ flies down (i.e., $p_{i,m}^{\text{D}} \Rightarrow p_{i,1}^{\text{D}}$), and we set $y = 1$. For the first chimney on Γ_{S}, ψ flies up on its DW side.

(2) Suppose that the last SP of c_i to be visited is p_a. When ψ flies from c_i to the next chimney, say, c_j, we pick an SP p_b from four candidate SPs of c_j by

$$p_b = \arg\min_{p_b \in \{p_{j,1}^{\text{D}}, p_{j,m}^{\text{D}}, p_{j,1}^{\text{U}}, p_{j,m}^{\text{U}}\}} \tilde{L}(p_a, p_b), \tag{22}$$

to minimize the path for ψ to fly from c_i to c_j.

Fig. 1(e) shows an example, where $m = 4$. The flight path is $p_0 \to p_{1,1}^{\text{D}} \to \cdots \to p_{1,4}^{\text{D}} \curvearrowright p_{1,4}^{\text{U}} \to p_{2,4}^{\text{D}} \to \cdots \to p_{2,1}^{\text{D}} \curvearrowright p_{2,1}^{\text{U}} \to p_{3,1}^{\text{U}} \curvearrowright p_{3,1}^{\text{D}} \to \cdots \to p_{3,4}^{\text{D}} \to p_0$. Evidently, ψ's flight direction and the locations of UW SPs may adaptively change. We give the maximum inter-chimney path length and flight length in AIS in Lemma 3 and Theorem 4, respectively.

Lemma 3. The maximum inter-chimney path length in AIS is $l_{AIS}^{IC} = (n-1)\sqrt{(\tilde{d}-2d_{MS})^2+\tilde{h}^2}+\beta_3$, where β_3 is the length sum of paths $p_0 \to p_{x_1,1}^{D}$ and $p_z \to p_0$. Here, p_z is the last SP to be visited at chimney c_{x_n} (i.e., the last chimney on Γ_{SP}).

Proof: In Fig. 1(e), the flight length between chimneys c_i and c_j is $\sqrt{\alpha_1^2+\alpha_2^2}$, where $\alpha_1 = \tilde{d}_{i,j} - 2d_{\text{MS}}$. By Eq. (22), p_a and p_b have the same height index[2], so their height difference (i.e., α_2) is $\tilde{h}_{i,j}$. Like the proof in Lemma 1, the maximum length of Γ_{IC} is $(n-1)\sqrt{(\tilde{d}-2d_{\text{MS}})^2+\tilde{h}^2}+\beta_3$. □

Theorem 4. In AIS, the maximum length of the flight path is $l_{AIS}^{IC} + n(\pi(r_{\max}+d_{MS})+(m-1)h_s)$.

Proof: Let us compare the flight paths in IUS and AIS, as shown in Fig. 1(d) and (e). For each chimney $c_i \in \hat{\mathcal{C}}$, UAV ψ does not need to fly on path $p_{i,m}^{\text{U}} \to \cdots \to p_{i,1}^{\text{U}}$, as there is only one UW SP in AIS. Thus, compared to IUS, the length of Γ_i is reduced by $(m-1)h_s$ in AIS. Based on Theorem 3 and Lemma 3, the maximum length of flight path in AIS is $l_{\text{AIS}}^{\text{IC}} + n(\pi(r_{\max}+d_{\text{MS}})+(m-1)h_s)$. □

5.5 Judgment on 3E-Chimneys

To check if a chimney c_i is a 3E-chimney, UAV ψ compares the EG concentration sampled at a DW SP p_d (denoted by ϑ_d) and that at a UW SP p_u (denoted by ϑ_u) for c_i. Specifically, ϑ_u can be viewed as c_i's ambient EG concentration (without c_i's effect), and ϑ_d is the sum of c_i's ambient EG concentration

2. If $p_a = p_{i,1}^{\text{U}}$, $p_b = p_{j,1}^{\text{D}}$ or $p_{j,1}^{\text{U}}$. If $p_a = p_{i,m}^{\text{U}}$, $p_b = p_{j,m}^{\text{D}}$ or $p_{j,m}^{\text{U}}$.

and the concentration of EG emitted from c_i. Hence, the EG concentration caused by c_i is $\vartheta_d - \vartheta_u$. Based on Eq. (1), we can deduce c_i's EG emission rate by

$$Q_i = \mu(\vartheta_d - \vartheta_u)/(\varphi_y \varphi_z B). \tag{23}$$

To calculate dilution factors φ_y and φ_z in Eq. (2), we employ p_d's coordinates as the reference and set the plume's height to $h = h_i + h_s$. Then, c_i is judged as a 3E-chimney if $Q_i > Q_{\mathtt{th}}$, where $Q_{\mathtt{th}}$ is the statutory threshold.

Generally speaking, a nearby chimney c_j on c_i's UW side can affect the EG concentration at c_i's UW SPs. If c_j emits much EG (i.e., 3E-chimney), the EG concentration sampled at c_i's UW SPs would be unusually high. On the contrary, if the difference between the EG concentration at c_i's UW SPs and the environmental EG concentration is small, c_j is very likely not a 3E-chimney. In this case, UAV ψ can skip c_j (for collecting its data) to reduce the flight path.

Suppose that c_j is the next chimney to c_i on path $\Gamma_{\mathtt{S}}$. If c_j is on c_i's UW side and $\tilde{d}_{i,j} \leq D_{\mathtt{th}}$, UAV ψ estimates c_j's EG emission rate after collecting data at all of c_i's UW SPs. Here, the condition $\tilde{d}_{i,j} \leq D_{\mathtt{th}}$ indicates that c_j is close enough to c_i, so the emission of EG by c_j has a great impact on the EG concentration at c_i's UW SPs. Given set $\hat{\mathcal{P}}_i^{\mathtt{U}}$ of c_i's UW SPs, let ϑ_k be the EG concentration sampled at each SP $p_{i,k}^{\mathtt{U}} \in \hat{\mathcal{P}}_i^{\mathtt{U}}$. Then, we can estimate c_j's EG emission rate as follows:

$$Q_j^{\mathtt{E}} = \min_{\forall p_{i,k}^{\mathtt{U}} \in \hat{\mathcal{P}}_i^{\mathtt{U}}} \left\{ \mu(\vartheta_k - \bar{\vartheta})/(\varphi_y \varphi_z B) \mid \varphi_y \varphi_z B > 0 \right\}, \tag{24}$$

where $\bar{\vartheta}$ is the environmental EG concentration[3]. When using ϑ_k to do calculations, we take $p_{i,k}^{\mathtt{U}}$'s coordinates as the reference for computing dilution factors φ_y and φ_z. In Eq. (24), the condition $\varphi_y \varphi_z B > 0$ ensures that the emission of EG by c_j is correlated with the EG concentration at SP $p_{i,k}^{\mathtt{U}}$. However, if no SP in $\hat{\mathcal{P}}_i^{\mathtt{U}}$ fulfills this condition, we set $Q_j^{\mathtt{E}} = \infty$, which means that c_j's EG emission rate cannot be estimated by using the EG concentration sampled at c_i's UW SPs. Then, UAV ψ infers that c_j is not a 3E-chimney if

$$Q_j^{\mathtt{E}} \leq Q_{\mathtt{th}} - Q_{\mathtt{adj}}, \tag{25}$$

where $Q_{\mathtt{adj}}$ is used to reflect the error of estimation in Eq. (24) and $Q_{\mathtt{adj}} < Q_{\mathtt{th}}/2$.

5.6 Design Rationale and Computational Complexity

Let us discuss the rationale of our path-planning framework. It creates path $\Gamma_{\mathtt{S}}$ via a TSP approximation solution to decide the sequence for UAV ψ to visit all chimneys in $\hat{\mathcal{C}}$. Then, we design four schemes to select SPs for each chimney, which is the framework's core. DLS aims to minimize ψ's flight path by picking two SPs for each chimney. Due to only a few SPs, the monitoring performance in DLS may be low. Thus, USS selects m pairs of DW/UW SPs for each chimney and lets ψ alternately collect data at DW and UW SPs, so the flight path around each chimney forms an upward spiral. However, these spirals lead to a long flight path. Hence, IUS asks ψ to visit DW SPs and then UW SPs to reduce the path length. AIS improves IUS by reducing UW SPs and shortening the path as ψ flies between chimneys. Hence, AIS can shorten the flight path without significantly degrading performance.

3. To obtain $\bar{\vartheta}$, UAV ψ can sample data at a location where there is no chimney nearby on the UW side of the industrial area.

When executing the monitoring task on a chimney, UAV ψ checks if the next chimney is obviously not a 3E-chimney (using the ISC3 model) at the same time. In this way, some chimneys can be removed from ψ's visiting list, which further reduces the flight path. Theorem 5 analyzes the time complexity of our path-planning framework.

Theorem 5. Let $T_{\mathtt{TSP}}(n)$ be the amount of time taken by a TSP approximation solution to find the shortest path to visit n nodes. The worst-case time complexity of our path-planning framework is $T_{\mathtt{TSP}}(n) + T_{\mathtt{SM}}$, where $T_{\mathtt{SM}} = O(n)$ if the DLS scheme is used to find SPs and $T_{\mathtt{SM}} = O(nm)$ otherwise.

Proof: In the path-planning framework, step 1 uses a TSP approximation solution to find path $\Gamma_{\mathtt{S}}$ to visit n chimneys in $\hat{\mathcal{C}}$, which takes $T_{\mathtt{TSP}}(n)$ time. In steps 2 and 3, UAV ψ flies to sample data at the SPs for each chimney c_i and uses Eq. (23) to compute its EG emission rate. Since DLS picks a pair of DW/UW SPs for c_i, it spends $O(1)$ time. On the other hand, USS, IUS, and AIS select m DW SPs for c_i, so they take $O(m)$ time to run steps 2 and 3. For step 4, ψ checks if the next chimney, say, c_j is not a 3E-chimney based on the data collected at c_i's UW SPs (i.e., $\hat{\mathcal{P}}_i^{\mathtt{U}}$). This is done by estimating c_j's EG emission rate $Q_j^{\mathtt{E}}$ using Eq. (24). Because DLS, USS, IUS, and AIS pick 1, m, m, and 1 UW SPs for c_i, they take $O(1)$, $O(m)$, $O(m)$, and $O(1)$ time to execute step 4. As $\hat{\mathcal{C}}$ contains n chimneys, $T_{\mathtt{SM}}$ is equal to $n(O(1) + O(1)) = O(n)$, $n(O(m) + O(m)) = O(nm)$, $n(O(m) + O(m)) = O(nm)$, $n(O(m) + O(1)) = O(nm)$ when DLS, USS, IUS, and AIS are respectively used. Hence, the theorem is proven. □

5.7 Distance to the Optimal Solution

We investigate the distance between each sampling scheme (i.e., a suboptimal solution) and the optimal solution. Let $\mathbf{L}_{\mathtt{X}}$ and $\mathbf{L}_{\mathtt{opt}}$ denote the flight lengths of a sampling scheme $\mathtt{X}$ and the optimal solution. The distance is defined as the maximum difference between $\mathbf{L}_{\mathtt{X}}$ and $\mathbf{L}_{\mathtt{opt}}$.

Like DLS, the optimal solution selects a pair of DW/UW SPs (with the same height) for each chimney $c_i \in \hat{\mathcal{C}}$. Suppose that no chimneys are excluded by step 4 in the path-planning framework. Then, the optimal solution has the same inter-chimney path (i.e, $\Gamma_{\mathtt{IC}}$) as DLS. Based on Eq. (4), the height of an SP for c_i in the optimal solution is $h_i + \Delta_{\mathrm{W}} + \Delta_{\mathrm{R}}$ (i.e., the plume's height). On the other hand, the height of an SP for c_i in DLS is $h_i + \Delta_{\mathtt{DLS}}$, where $\Delta_{\mathtt{DLS}} = h_s, -h_s$, or 0. Hence, to sample data at two SPs $p_{i,1}^{\mathtt{D}}$ and $p_{i,1}^{\mathtt{U}}$ for a chimney c_i, the maximum difference between the flight lengths in the optimal solution and DLS is $2(\Delta_{\mathrm{W}} + \Delta_{\mathrm{R}} + h_s)$. Since $\hat{\mathcal{C}}$ has n chimneys, the distance between DLS and the optimal solution is $2n(\gamma + h_s)$, where $\gamma = \max\{\Delta_{\mathrm{W}} + \Delta_{\mathrm{R}} \mid \forall c_i \in \hat{\mathcal{C}}\}$.

To obtain the distance for USS, IUS, and AIS, we compute the maximum gap between the flight lengths in each sampling scheme and DLS. For convenience, we denote this as $\mathbf{L}_{\mathtt{X}} - \mathbf{L}_{\mathtt{DLS}}$. Besides, we set $\pi(r_{\max} + d_{\mathtt{MS}}) = \Phi$.

For USS, based on Theorems 2 and 1, we obtain that $\mathbf{L}_{\mathtt{USS}} - \mathbf{L}_{\mathtt{DLS}} = (l_{\mathtt{USS}}^{\mathtt{IC}} + mn\sqrt{h_s^2 + 4\Phi^2}) - (l_{\mathtt{DLS}}^{\mathtt{IC}} + n\Phi) = l_{\mathtt{USS}}^{\mathtt{IC}} - l_{\mathtt{DLS}}^{\mathtt{IC}} + n(m\sqrt{h_s^2 + 4\Phi^2} - \Phi)$. Thus, the distance between USS and the optimal solution is $l_{\mathtt{USS}}^{\mathtt{IC}} - l_{\mathtt{DLS}}^{\mathtt{IC}} + n(m\sqrt{h_s^2 + 4\Phi^2} - \Phi) + 2n(\gamma + h_s)$.

For IUS, according to Theorems 3 and 1, we can derive that $\mathbf{L}_{\mathtt{IUS}} - \mathbf{L}_{\mathtt{DLS}} = (l_{\mathtt{DLS}}^{\mathtt{IC}} + n(\Phi + 2(m-1)h_s)) - (l_{\mathtt{DLS}}^{\mathtt{IC}} + n\Phi) =$

TABLE 3: Simulation parameters.

Environmental parameters:	
area size	$2\,\text{km} \times 2\,\text{km}$
ambient temperature (T_a)	25°C
wind speed (μ)	1 m/s
EG type	CO_2 (concentration: $\bar{\vartheta} = 400\,\text{ppm}$)
molecular weight	air: $29\,\text{g/m}^3$, EG: $44\,\text{g/m}^3$
Chimney-related parameters:	
number	20, 40, 60, 80, 100
height (h_i)	25 m or 30 m
radius (r_i)	0.5 m or 1 m
EG temperature (T_s)	30°C
GEV (v_i)	2 m/s or 3 m/s
EG emission rate (Q_i)	50,000∼500,000 mg/s
Parameters of sampling schemes:	
minimum safe distance (d_{MS})	5 m
interval between SPs (h_s)	1 m
number of SP pairs (m)	20
statutory threshold (Q_{th})	400,000 mg/s
Q_{adj} in Eq. (25)	130,000 mg/s

$2n(m-1)h_s$. Thus, the distance between IUS and the optimal solution is $2n(m-1)h_s + 2n(\gamma + h_s) = 2n(mh_s + \gamma)$.

For AIS, with both Theorems 4 and 1, we derive that $\mathbf{L}_{\text{AIS}} - \mathbf{L}_{\text{DLS}} = (l^{\text{IC}}_{\text{AIS}} + n(\Phi + (m-1)h_s)) - (l^{\text{IC}}_{\text{DLS}} + n\Phi) = l^{\text{IC}}_{\text{AIS}} - l^{\text{IC}}_{\text{DLS}} + n(m-1)h_s$. Hence, the distance between AIS and the optimal solution is $l^{\text{IC}}_{\text{AIS}} - l^{\text{IC}}_{\text{DLS}} + n(m-1)h_s + 2n(\gamma + h_s) = l^{\text{IC}}_{\text{AIS}} - l^{\text{IC}}_{\text{DLS}} + n(2\gamma + (m+1)h_s)$.

6 Simulation Study

Our simulation is written in C++. Table 3 lists parameters. We consider a $2\,\text{km} \times 2\,\text{km}$ industrial area with some chimneys randomly distributed. For the Pasquill stability category, class E (i.e., slightly stable) is used, where the ambient temperature is 25°C. Wind blows along the X-axis with a speed of 1 m/s. We choose CO_2 as EG, whose environmental concentration is 400 ppm. The molecular weights of air and EG are $29\,\text{g/m}^3$ and $44\,\text{g/m}^3$, respectively.

To study the effect of chimney density, we raise the number of chimneys from 20 to 100. For each chimney, its height is 25 m or 30 m, and its radius is 0.5 m or 1 m. Hence, there are four types of chimneys with different heights and radii. The temperature of EG emitted from chimneys is 30°C. Though both GEV (affecting the plume's height) and EG emission rate (used for 3E-chimney judgment) are given in Table 3, these two parameters are unknown when scheduling the flight path and finding SPs for a UAV.

To avoid being damaged, the UAV has to keep a chimney away from at least 5 m (i.e., the minimum safe distance d_{MS}). For the USS, IUS, and AIS schemes, we set $m = 20$ for each chimney (i.e., 20 pairs of DW/UW SPs), where the interval h_s between SPs is 1 m. The statutory threshold (i.e., Q_{th}) is set at 400,000 mg/s. If a chimney's EG emission rate exceeds Q_{th}, it is a 3E-chimney. Moreover, Q_{adj} is set to 130,000 mg/s to reflect the error of estimation in Eq. (24).

The TSP approximation solution in [38] is used to find the shortest path Γ_{S} to visit all chimneys. We evaluate the cost and performance of different sampling schemes. As mentioned in Section 4, the cost is defined as the length of the flight path, and the performance is assessed via the metrics of accuracy, recall, precision, and F1-score. We also choose IGBA [31], a cutting-edge solution to find 3E-chimneys, for comparison. As discussed in Section 3.3, IGBA relies on the knowledge of the GEV (i.e., v_i) of each chimney to get the correct heights of SPs. In practice, GEV is an unknown parameter, so we set v_i to 2.5 m/s (i.e., the average GEV of chimneys). Besides, we give the optimal solution as a reference for comparison. It picks two SPs for each chimney based on the plume's height. Evidently, the optimal solution is theoretical, as the plume's height cannot be known. In addition to cost and performance, we also study the effects of the mechanism to skip chimneys (discussed in Section 5.5) and some parameters. In each experiment, we repeat the simulation 100 times and take the average.

6.1 Comparison of Cost

Fig. 2(a) gives the path length using different schemes. The path length increases with more chimneys since the UAV has to collect data at more SPs. IGBA and DLS have a path length similar to the optimal solution, as they pick two SPs for each chimney. USS results in a much longer path length than others, and its length increases rapidly when the number of chimneys grows. That is because USS asks the UAV to spiral upward at each chimney to sample data. As analyzed in Theorem 2, doing so significantly lengthens the flight path. IUS lets the UAV fly in an inverted-U shape to avoid spirals, thereby greatly reducing path length. As can be seen, the difference between IUS's length and the lengths of IGBA, DLS, and the optimal solution is small. By decreasing UW SPs, AIS can reduce the path length as compared to IUS.

Using the optimal solution as a benchmark, the percentage increase in path length by a scheme X is $\frac{\mathbf{L}_{\text{X}} - \mathbf{L}_{\text{opt}}}{\mathbf{L}_{\text{opt}}} \times 100\%$, where $\mathbf{L}_{\text{X}}$ and $\mathbf{L}_{\text{opt}}$ denote the path lengths of scheme X and the optimal solution. A lower percentage increase means that scheme X requires a lower cost. On average, IGBA, DLS, USS, IUS, and AIS have percentage increases of 0.07%, 0.09%, 279.37%, 18.43%, and 3.68%. This result reveals that IGBA, DLS, and AIS can efficiently save on monitoring costs.

Fig. 2(b) shows the number of SPs chosen to collect data. The more chimneys there are, the more SPs are selected. In general, IGBA, DLS, and the optimal solution choose two SPs for each chimney (excluding those chimneys skipped), so they have a similar number of SPs. USS and IUS select m pairs of DW/UW SPs for each chimney. However, USS lets the UAV check if the current chimney c_i is a 3E-chimney whenever it has sampled data at each pair of DW/UW SPs. If so, the UAV leaves c_i and flies to the next chimney. In IUS, the UAV has to visit all DW SPs of each chimney (that is, only some UW SPs can be skipped). Hence, IUS picks more SPs than USS. Despite this, IUS has a much shorter path than USS (referring to Fig. 2(a)), as the spiral flight in USS makes the flight path pretty long. AIS selects m DW SPs and one UW SP for each chimney, so it has fewer SPs than USS and IUS.

6.2 Comparison of Performance

Fig. 2(c) gives the accuracy of each scheme, which indicates the proportion of true positives and true negatives (i.e., right answers) as defined in Eq. (9). Both IGBA and DLS select only two SPs for each chimney. Without knowing the correct plume's height at each chimney, their accuracy is below 0.83. On the other hand, USS, IUS, and AIS perform almost as well in accuracy. Since they pick enough DW SPs for sampling data, even if the plume's height cannot be known, the accuracy of these three schemes can stay above 0.90.

In Fig. 2(d), we measure the recall of each scheme. Based on Eq. (10), the recall cares about whether there is a miss without considering false alarms. The recall of IGBA and DLS is lower

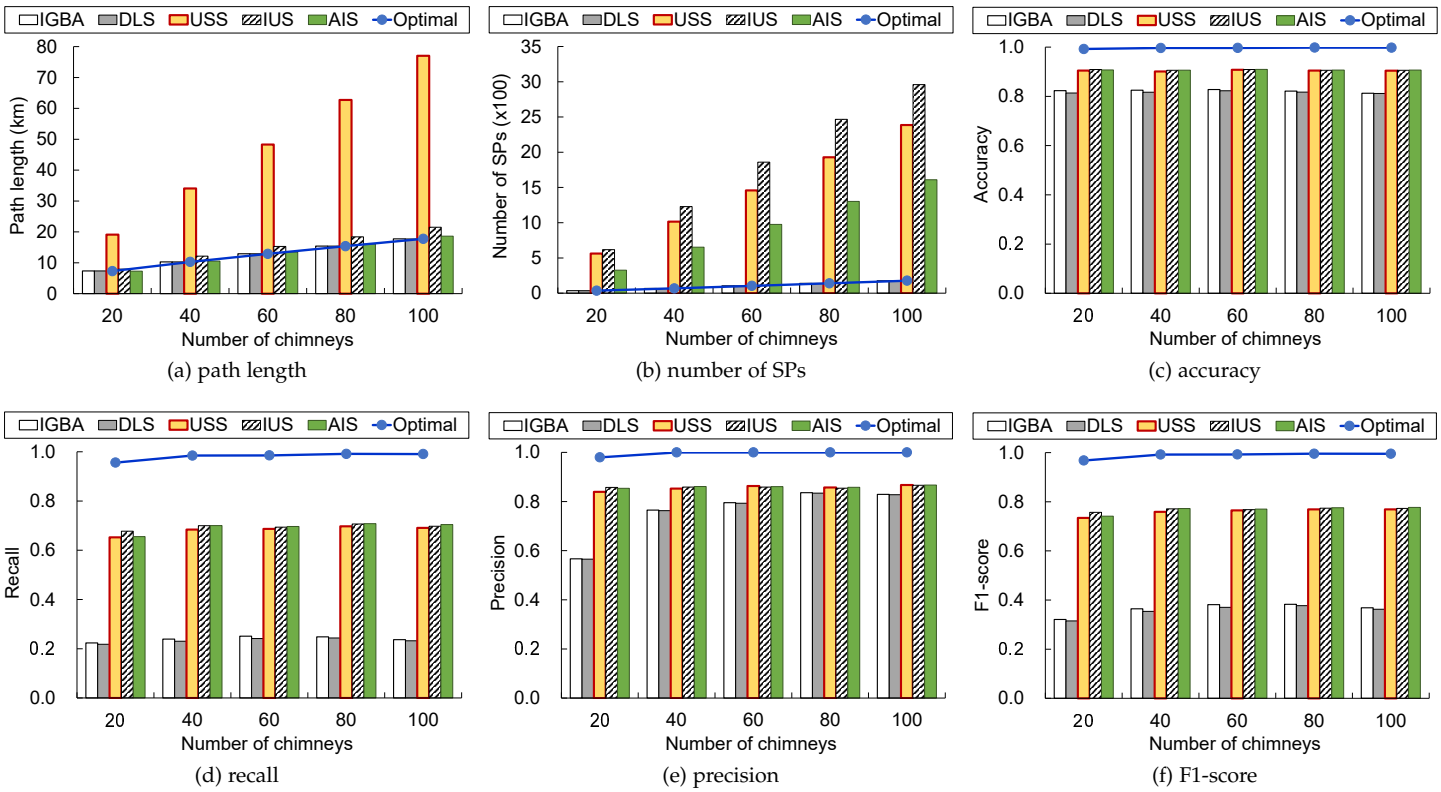

Fig. 2: Comparison of the monitoring cost and performance.

TABLE 4: Performance reduction percentage for each scheme.

metric	IGBA	DLS	USS	IUS	AIS
accuracy	17.50%	18.06%	9.20%	8.97%	8.92%
recall	75.59%	76.26%	30.50%	29.18%	29.42%
precision	23.84%	24.02%	14.05%	13.73%	13.65%
F1-score	63.24%	64.03%	23.21%	22.28%	22.40%

than 0.25, meaning that many 3E-chimneys are missed. On the contrary, the recall of IUS, USS, and AIS is close to 0.70. The result reveals that they can identify much more 3E-chimneys than IGBA and DLS.

Then, Fig. 2(e) compares the precision of different schemes. Unlike the recall, the precision pays attention to false positives (referring to Eq. (11)). In IGBA and DLS, the precision rises as the number of chimneys grows, where the maximum precision is 0.836. On the other hand, the precision of USS, IUS, and AIS is stable and stays above 0.85. This implies that USS, IUS, and AIS can efficiently reduce false positives, as compared to IGBA and DLS, especially with fewer chimneys.

Fig. 2(f) gives the F1-score of each scheme. According to Eq. (12), the F1-score considers both recall and precision. The maximum F1-score in IGBA and DLS is 0.3826 (due to their low recall). For USS, IUS, and AIS, their average F1-scores are 0.7593, 0.7686, and 0.7674, respectively. Evidently, they perform much better than IGBA and DLS.

In Fig. 2(c)–(f), the accuracy, recall, precision, and F1-score of the optimal solution are close to one but lower than one. These slight differences are caused by skipping chimneys. The details will be discussed later in Section 6.3.

Let $\mathbf{M}_{\mathtt{X}}$ and $\mathbf{M}_{\mathtt{opt}}$ denote the values of a performance metric (i.e., accuracy, recall, precision, and F1-score) in a scheme $\mathtt{X}$ and the optimal solution. Taking the optimal solution as a benchmark, the performance reduction percentage of scheme $\mathtt{X}$ is $\frac{\mathbf{M}_{\mathtt{opt}}-\mathbf{M}_{\mathtt{X}}}{\mathbf{M}_{\mathtt{opt}}} \times 100\%$. A lower performance reduction percentage implies that scheme $\mathtt{X}$ performs better in that metric. Table 4 presents the performance reduction percentages of different schemes. Since IGBA and DLS let the UAV sample data at only two SPs for each chimney, they perform the worst in all metrics. The performance of AIS is not much different from that of USS and IUS, which means that it is safe for AIS to reduce UW SPs. According to the discussion in Section 6.1 and the result in Table 4, we conclude that AIS can strike a good balance between monitoring cost and performance as compared to other schemes.

6.3 Effect of Skipping Chimneys

As mentioned in Section 5.5, after the UAV samples data at UW SPs of a chimney c_i, it also estimates the EG emission rate $Q_j^{\mathtt{E}}$ of another chimney c_j using Eq. (24), where c_j meets three conditions: 1) c_j is the next chimney on path $\Gamma_{\mathtt{S}}$; 2) c_j is located on c_i's UW side; and 3) the distance between c_i and c_j is below $D_{\mathtt{th}}$ (i.e., $\tilde{d}_{i,j} \leq D_{\mathtt{th}}$). If $Q_j^{\mathtt{E}}$ satisfies the condition in Eq. (25), the UAV infers that c_j is not a 3E-chimney and thereby skips c_j. In the simulation, we set $D_{\mathtt{th}}$ to 300 m.

Fig. 3(a) shows the percentage of chimneys skipped. When the density of chimneys is low (i.e., 20 chimneys), the distance between two chimneys is large. So, the condition $\tilde{d}_{i,j} \leq D_{\mathtt{th}}$ is relatively difficult to achieve. On the other hand, when the density of chimneys is high (e.g., 80 chimneys or more), the EG concentration sampled at c_i's UW SPs is more susceptible to other 3E-chimneys. In other words, c_j becomes less likely to be judged as not a 3E-chimney. Hence, this percentage first increases and then decreases as the number of chimneys grows. The peak of each scheme occurs with 40 and 60 chimneys.

In Fig. 3(a), since the optimal solution, DLS, and AIS let the UAV sample data at only one UW SP for each chimney, their

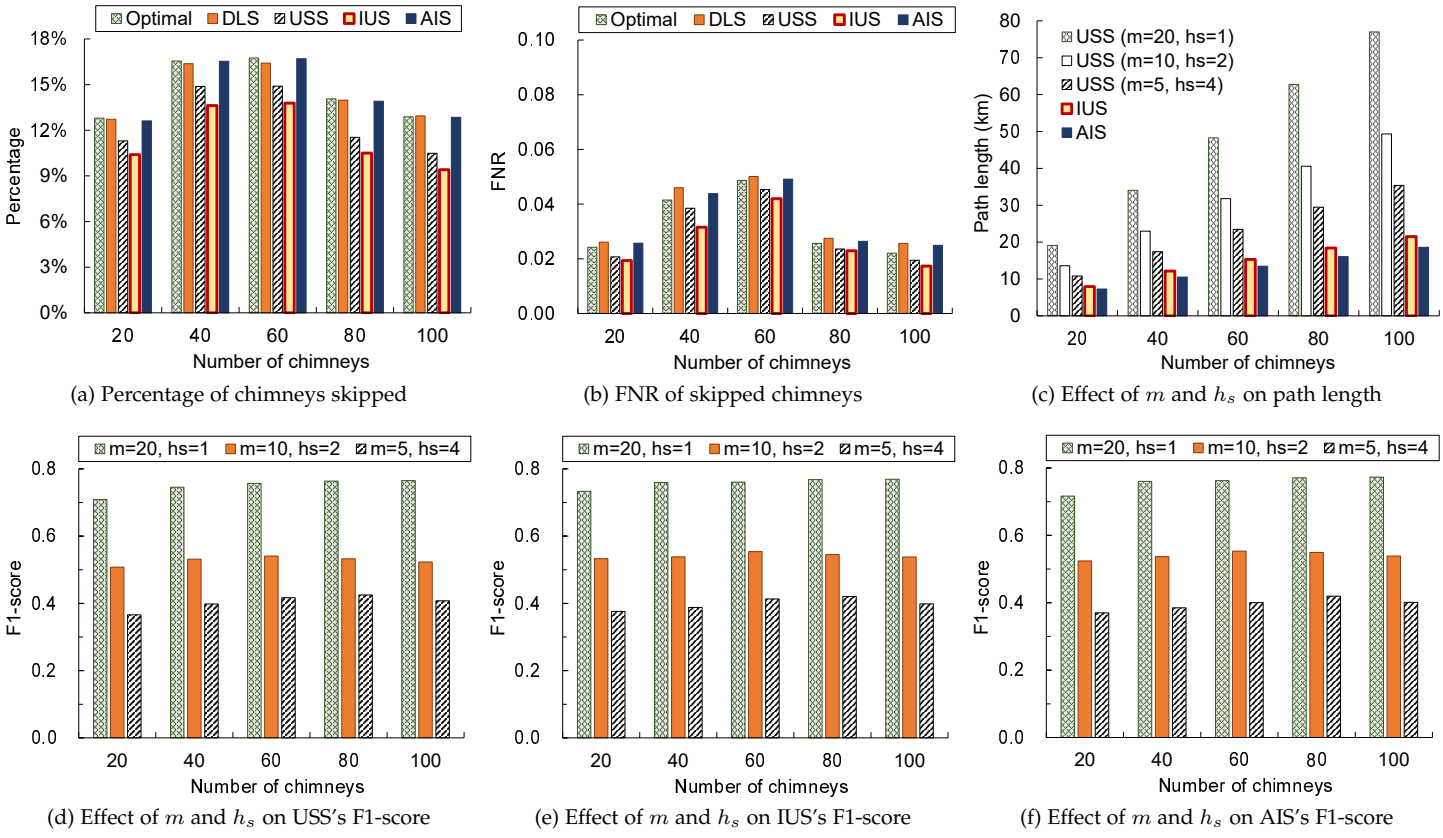

(a) Percentage of chimneys skipped (b) FNR of skipped chimneys (c) Effect of m and h_s on path length

(d) Effect of m and h_s on USS's F1-score (e) Effect of m and h_s on IUS's F1-score (f) Effect of m and h_s on AIS's F1-score

Fig. 3: Effects of skipping chimneys and parameters.

percentages are high (i.e., 12.6%–16.8%). Both USS and IUS choose m UW SPs for each chimney. Due to the calculation of Q_j^{E} by Eq. (24), it becomes relatively difficult for Q_j^{E} to meet the condition in Eq. (25). That explains why both USS and IUS have lower percentages. Moreover, USS lets the UAV sample data at fewer UW SPs than IUS (referring to Fig. 2(b)). Hence, more chimneys are skipped in USS than in IUS. Specifically, USS skips 10.5%–14.9% of chimneys, while IUS skips only 9.4%–13.8% of chimneys.

In the path-planning framework, only when c_j is obviously not a 3E-chimney can c_j be skipped. Hence, we are concerned about false negatives, where a false negative occurs when c_j is judged as not a 3E-chimney, but c_j actually is. Fig. 3(b) shows the *false negative rate (FNR)* of skipped chimneys, whose trend is similar to that in Fig. 3(a). When more chimneys are skipped, the FNR increases accordingly. Observing Fig. 3(b), the FNR stays below 0.05 for all schemes. This result reveals that our proposed ISC3-based mechanism to skip chimneys in Section 5.5 is accurate.

6.4 Effect of Parameters

For each chimney, USS and IUS select m pairs of DW/UW SPs and AIS picks m UW SPs. Besides, the distance between two adjacent SPs is h_s. Hence, we study the effect of m and h_s on the cost and performance of USS, IUS, and AIS. Three combinations are considered: $(m, h_s) = (20, 1)$, $(10, 2)$, and $(5, 4)$. Therefore, the sampling altitude range for each chimney can be kept at $m \times h_s = 20$.

Fig. 3(c) shows the effect of m and h_s on path length. In IUS and AIS, the UAV flies along a beeline to visit all DW (or UW) SPs of each chimney, as shown in Fig. 1(d) and (e). Since the sampling altitude range stays the same, changing m and h_s has no effect on path length in IUS and AIS. Thus, in Fig. 3(c), we only show the result of IUS and AIS by setting $(m, h_s) = (20, 1)$. On the contrary, changing m and h_s has a great impact on path length in USS, because USS makes the UAV fly on an upward spiral to collect data. Based on Theorem 2, the length of a spiral can be significantly decreased by reducing m, thereby shortening the UAV's flight path. Despite this, USS's path length is still longer than that of IUS and AIS.

In Fig. 3(d), (e), and (f), we present the effect of m and h_s on the F1-scores of USS, IUS, and AIS, respectively. As can be seen, reducing m (and raising h_s) decreases F1-scores, as the UAV samples data at fewer SPs for each chimney. This result shows that using a large m value (i.e., increasing the number SPs) can help improve monitoring performance.

7 Prototyping Experience

To show the feasibility of our path-planning framework, we made a prototype system to measure the concentration of CO_2 gases emitted from small chimneys in a micro-field, as shown in Fig. 4(a). Nine 12-inch computer fans are used to generate a steady airflow, where the wind blows along the X-axis and has a speed of 1 m/s. Acrylic tubes are used to simulate chimneys. The radius of a chimney is 0.5 cm, and its height can be 20 cm or 30 cm. Each chimney is connected to the CO_2 gas cylinder (i.e., the EG source) through an air pipe, where its EG emission can be adjusted using a control valve.

To implement the UAV, one Arduino board [39] is used to integrate a CO_2 sensor and an XBee module [40], as shown in Fig. 4(b). The CO_2 sensor uses non-dispersive infrared and

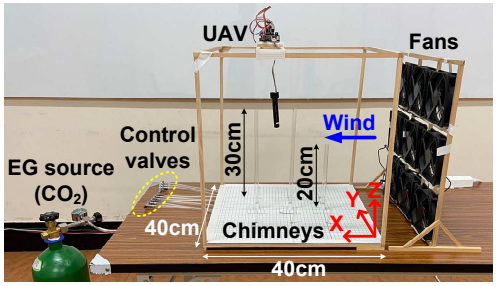

(a) Snapshot of the prototype system

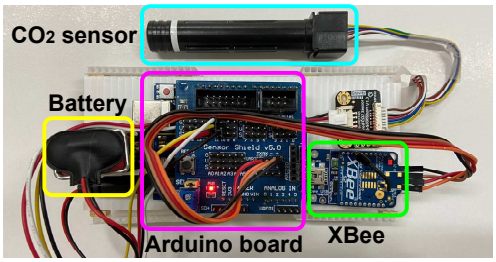

(b) Components of the UAV

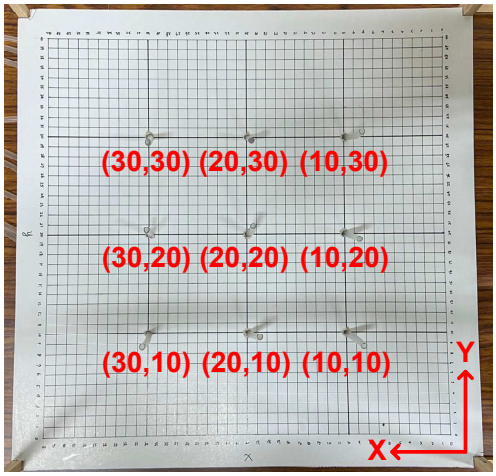

(c) Micro-field and the coordinates of chimneys

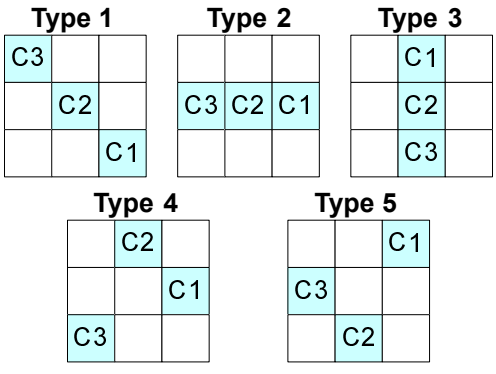

(d) Placement of chimneys

Fig. 4: A prototype system for identifying 3E-chimneys.

has an effective range of 0–50000 ppm. The XBee module offers low-powered ZigBee communications, and its communication range is at most 120 m. The UAV glides along tracks to check out each chimney. Besides, the CO_2 sensor can be hung down to collect data at different heights.

Fig. 4(c) gives the micro-field and the coordinates of chimneys. The micro-field is a 40 cm×40 cm square where nine locations are placed with outlets for air pipes. We select three locations from them to place chimneys. There are five types of chimney placement, as Fig. 4(d) shows. Chimney C1 is a 3E-chimney whose GEV is 2 m/s. The GEV of chimney C2 is 0.1 m/s. Chimney C3 does not discharge CO_2. In other words, C2 and C3 are not 3E-chimneys. Moreover, we consider three cases for chimney height: 1) the height of every chimney is 30 cm; 2) C1's height is 30 cm and other chimneys have a height of 20 cm; and 3) C1's height is 20 cm and other chimneys have a height of 30 cm. Hence, there are 5 (placement) × 3 (height) combinations. We conduct 15 experiments, where each experiment uses a different combination of placement and height. Each experiment is repeated 30 times.

TABLE 5: Performance of different schemes using the prototype.

metric	IGBA	DLS	USS	IUS	AIS
accuracy	0.9444	0.93333	0.9704	0.9733	0.9726
recall	0.9000	0.86667	1.0000	1.0000	1.0000
precision	0.9310	0.92857	0.9184	0.9259	0.9240
F1-score	0.9153	0.89655	0.9574	0.9615	0.9605

Since the ISC3 model considers large-scale fields, we cannot use Eq. (23) to deduce a chimney's EG emission rate based on the EG concentration sampled at its DW and UW SPs (i.e., ϑ_d and ϑ_u). Instead, we check if $\vartheta_d - \vartheta_u > 5000$ ppm. If so, the chimney is inferred to be a 3E-chimney. Besides, we do not use the mechanism in Section 5.5 to skip chimneys. Hence, the UAV collects data at every chimney for judgment. For the USS, IUS, and AIS schemes, we set $m = 3$ and $h_s = 2$ cm. In other words, each chimney has three pairs of DW/UW SPs and the distance between two adjacent SPs is 2 cm.

Table 5 compares the performance of IGBA and our four proposed sampling schemes (i.e., DLS, USS, IUS, and AIS) by conducting experiments using the prototype. In IGBA, we set $v_i = 2$ m/s (i.e., the GEV of a 3E-chimney). Since IGBA guesses chimney C1's GEV correctly, it performs better than DLS. However, IGBA and DLS pick only a pair of DW/UW SPs to collect data for each chimney, so their performance is not good compared to other schemes. On the other hand, USS, IUS, and AIS perform similarly, where they can recognize 3E-chimneys more efficiently, especially in recall and F1-score. This phenomenon illustrates the need to select multiple pairs of SPs for each chimney, which helps reduce false positives and false negatives.

8 Conclusion

Air pollution is one serious problem, and finding pollution sources is a challenge. This paper searched 3E-chimneys in an industrial area using UAVs. We proposed the path-planning framework to schedule a UAV's flight path and choose SPs around each chimney for the UAV to collect data. Specifically, the shortest path was created to visit chimneys. We designed the DLS, USS, IUS, and AIS schemes to select suitable SPs. On executing the monitoring task, the UAV checked if the next chimney was not a 3E-chimney by the ISC3 model. If so, the UAV skipped that chimney to reduce the flight path. Through simulations, we showed that USS, IUS, and AIS performed better than IGBA, a cutting-edge method to find 3E-chimneys, especially in recall and F1-score. AIS had a shorter flight path than USS and IUS, so it better balanced cost and performance. In addition, we developed a prototype system to measure the concentration of CO_2 gases emitted from small chimneys in a micro-field to demonstrate the viability of our framework.

For future work, the warden issue mentioned in Remark 2 deserves further investigation. UAVs conduct covert communications based on the partial location information of a warden. In this case, the flight path of a UAV needs to be adjusted to not only collect data from the selected SPs but also prevent the warden from detecting its data transmissions.

REFERENCES

[1] World Health Organization, "Air pollution." [Online]. Available: https://www.who.int/health-topics/air-pollution

[2] Y.C. Wang, "Mobile solutions to air quality monitoring," in *Mobile Solutions and Their Usefulness in Everyday Life*. Heidelberg: Springer, 2019, pp. 225–249.

[3] M. Mozaffari, W. Saad, M. Bennis, Y.H. Nam, and M. Debbah, "A tutorial on UAVs for wireless networks: Applications, challenges, and open problems," *IEEE Comm. Surveys & Tutorials*, vol. 21, no. 3, pp. 2334–2360, 2019.

[4] Z. Wei, M. Zhu, N. Zhang, L. Wang, Y. Zou, Z. Meng, H. Wu, and Z. Feng, "UAV-assisted data collection for Internet of Things: A survey," *IEEE Internet of Things J.*, vol. 9, no. 17, pp. 15460–15483, 2022.

[5] U.S. Environmental Protection Agency, *Industrial Source Complex (ISC) Dispersion Model User's Guide*. Columbus: BiblioGov Publishing, 2013.

[6] Air Resources Laboratory, "Pasquill stability classes." [Online]. Available: https://www.ready.noaa.gov/READYpgclass.php

[7] B. Montrucchio, E. Giusto, M.G. Vakili, S. Quer, R. Ferrero, and C. Fornaro, "A densely-deployed, high sampling rate, open-source air pollution monitoring WSN," *IEEE Trans. Vehicular Technology*, vol. 69, no. 12, pp. 15786–15799, 2020.

[8] X. Li, M. Sun, Y. Ma, L. Zhang, Y. Zhang, R. Yang, and Q. Liu, "Using sensor network for tracing and locating air pollution sources," *IEEE Sensors J.*, vol. 21, no. 10, pp. 12162–12170, 2021.

[9] A. Boubrima, W. Bechkit, and H. Rivano, "Optimal WSN deployment models for air pollution monitoring," *IEEE Trans. Wireless Comm.*, vol. 16, no. 5, pp. 2723–2735, 2017.

[10] C. Sun, Y. Yu, V.O.K. Li, and J.C.K. Lam, "Multi-type sensor placements in Gaussian spatial fields for environmental monitoring," *Sensors*, vol. 19, no. 1, pp. 1–19, 2019.

[11] S. Ameer, M.A. Shah, A. Khan, H. Song, C. Maple, S.U. Islam, and M.N. Asghar, "Comparative analysis of machine learning techniques for predicting air quality in smart cities," *IEEE Access*, vol. 7, pp. 128325–128338, 2019.

[12] K. Matovic and N. Vlahovic, "Air quality prediction in smart city," *Proc. Int'l Conf. Advanced Technologies, Systems and Services in Telecomm.*, 2021, pp. 287–290.

[13] Y.C. Wang, "Mobile sensor networks: System hardware and dispatch software," *ACM Computing Surveys*, vol. 47, no. 1, pp. 12:1–12:36, 2014.

[14] X. Cheng, B. He, G. Li, and B. Cheng, "A survey of crowdsensing and privacy protection in digital city," *IEEE Trans. Computational Social Systems*, pp. 1–17, 2023.

[15] J. Dutta, C. Chowdhury, S. Roy, A.I. Middya, and F. Gazi, "Towards smart city: Sensing air quality in city based on opportunistic crowdsensing," *Proc. Int'l Conf. Distributed Computing and Networking*, 2017, pp. 1–6.

[16] M.A. Fekih, W. Bechkit, H. Rivano, M. Dahan, F. Renard, L. Alonso, and F. Pineau, "Participatory air quality and urban heat islands monitoring system," *IEEE Trans. Instrumentation and Measurement*, vol. 70, pp. 1–14, 2021.

[17] T.H. Frampton, A. Tiele, and J.A. Covington, "Development of a personalised environmental quality monitoring system (PONG)," *IEEE Sensors J.*, vol. 21, no. 13, pp. 15230–15236, 2021.

[18] T. Liu, Y. Zhu, Y. Yang, and F. Ye, "ALC^2: When active learning meets compressive crowdsensing for urban air pollution monitoring," *IEEE Internet of Things J.*, vol. 6, no. 6, pp. 9427–9438, 2019.

[19] S. Devarakonda, P. Sevusu, H. Liu, R. Liu, L. Iftode, and B. Nath, "Real-time air quality monitoring through mobile sensing in metropolitan areas," *Proc. ACM SIGKDD Int'l Workshop on Urban Computing*, 2013, pp. 1–8.

[20] K. Hu, V. Sivaraman, B.G. Luxan, and A. Rahman, "Design and evaluation of a metropolitan air pollution sensing system," *IEEE Sensors J.*, vol. 16, no. 5, pp. 1448–1459, 2016.

[21] D. Zhang and S.S. Woo, "Real time localized air quality monitoring and prediction through mobile and fixed IoT sensing network," *IEEE Access*, vol. 8, pp. 89584–89594, 2020.

[22] S.C. Hu, Y.C. Wang, C.Y. Huang, and Y.C. Tseng, "Measuring air quality in city areas by vehicular wireless sensor networks," *J. Systems and Software*, vol. 84, no. 11, pp. 2005–2012, 2011.

[23] Y.C. Wang and G.W. Chen, "Efficient data gathering and estimation for metropolitan air quality monitoring by using vehicular sensor networks," *IEEE Trans. Vehicular Technology*, vol. 66, no. 8, pp. 7234–7248, 2017.

[24] X. Chen, S. Xu, X. Liu, X. Xu, H.Y. Noh, L. Zhang, and P. Zhang, "Adaptive hybrid model-enabled sensing system (HMSS) for mobile fine-grained air pollution estimation," *IEEE Trans. Mobile Computing*, vol.21, no.6, pp. 1927–1944, 2022.

[25] S. Duangsuwan and P. Jamjareekulgarn, "Development of drone real-time air pollution monitoring for mobile smart sensing in areas with poor accessibility," *Sensors and Materials*, vol. 32, no. 2, pp. 511–520, 2020.

[26] J. Gao, Z. Hu, K. Bian, X. Mao, and L. Song, "AQ360: UAV-aided air quality monitoring by 360-degree aerial panoramic images in urban areas," *IEEE Internet of Things J.*, vol. 8, no. 1, pp. 428–442, 2021.

[27] Y. Yang, Z. Zheng, K. Bian, L. Song, and Z. Han, "Real-time profiling of fine-grained air quality index distribution using UAV sensing," *IEEE Internet of Things J.*, vol. 5, no. 1, pp. 186–198, 2018.

[28] P. Chhikara, R. Tekchandani, N. Kumar, M. Guizani, and M.M. Hassan, "Federated learning and autonomous UAVs for hazardous zone detection and AQI prediction in IoT environment," *IEEE Internet of Things J.*, vol. 8, no. 20, pp. 15456–15467, 2021.

[29] Z. Hu, Z. Bai, Y. Yang, Z. Zheng, K. Bian, and L. Song, "UAV aided aerial-ground IoT for air quality sensing in smart city: Architecture, technologies, and implementation," *IEEE Network*, vol. 33, no. 2, pp. 14–22, 2019.

[30] M.A. Hoque, M. Hossain, S. Noor, S.M.R. Islam, and R. Hasan, "IoTaaS: Drone-based Internet of Things as a service framework for smart cities," *IEEE Internet of Things J.*, vol. 9, no. 14, pp. 12425–12439, 2022.

[31] V.V. Le, D.H.P. Nguyen, H.D. Wang, B.H. Liu, and S.I. Chu, "Efficient UAV scheduling for air pollution source detection from chimneys in an industrial area," *IEEE Sensors J.*, vol. 22, no. 20, pp. 19983–19994, 2022.

[32] Y. Li and M. Xia, "Ground-to-air communications beyond 5G: A coordinated multipoint transmission based on Poisson-Delaunay triangulation," *IEEE Trans. Wireless Comm.*, vol. 22, no. 3, pp. 1841–1854, 2023.

[33] Y.C. Wang and S. Lee, "Small-cell planning in LTE HetNet to improve energy efficiency," *Int'l J. Comm. Systems*, vol. 31, no. 5, pp. 1–18, 2018.

[34] X. Chen, M. Sheng, N. Zhao, W. Xu, and D. Niyato, "UAV-relayed covert communication towards a flying warden," *IEEE Trans. Comm.*, vol. 69, no. 11, pp. 7659–7672, 2021.

[35] B. Yang, T. Taleb, G. Chen, and S. Shen, "Covert communication for cellular and X2U-enabled UAV networks with active and passive wardens," *IEEE Network*, vol. 36, no. 1, pp. 166–173, 2022.

[36] D. Davendra, *Traveling Salesman Problem, Theory and Applications*. London: IntechOpen, 2010.

[37] Y.C. Wang, C.C. Hu, and Y.C. Tseng, "Efficient placement and dispatch of sensors in a wireless sensor network," *IEEE Trans. Mobile Computing*, vol. 7, no. 2, pp. 262–274, 2008.

[38] B. Wei, Y. Xing, X. Xia, and L. Ling, "A novel particle swarm optimization with genetic operator and its application to TSP," *Int'l J. Cognitive Informatics and Natural Intelligence*, vol. 15, no. 4, pp. 1–17, 2021.

[39] Arduino Documentation. [Online]. Available: https://docs.arduino.cc/

[40] DiGi XBee. [Online]. Available: https://www.digi.com/products/embedded-systems/digi-xbee